LASNEX—A 2-D Physics Code for Modeling ICF

J. A. Harte

W. E. Alley

D. S. Bailey

J. L. Eddleman

G. B. Zimmerman

Introduction

The LASNEX computer code was developed to study inertial confinement fusion (ICF), to design ICF experiments, and to analyze the results. The code has evolved over time and been greatly enhanced with improved physics and modern computer science tools. LASNEX was first referred to in the literature in 1972[1] and first documented in 1975.[2]

This article presents an overview of the code, describing the physics models, the code structure, the methods used to solve the equations, and the user interface, providing supplemental information and updates to the previous review article published in 1980.[3] Although the general structure of the physics in the code is very much the same, many improvements have been added since 1980. For instance, the user interface has been greatly enhanced by the addition of the Basis code development system.[4] In addition, the code has been improved in response to requests, suggestions, and feedback from its users, who often challenge its capabilities to a far greater degree than the code developers do. The success of LASNEX as an important scientific tool is due to the team effort of the code developers and its users.

LASNEX models in two dimensions by assuming axial symmetry. It represents the spatial variation of its many physical quantities, such as temperature, density or pressure, on a two-dimensional (2-D), axially symmetric mesh composed of arbitrarily shaped quadrilaterals. LASNEX evolves the hydrodynamics and follows the electron, ion, and radiation heat conduction, and the coupling among these energy fields. There are many possible sources and boundary conditions that can be imposed on a LASNEX simulation, which can vary both in time and space. The possible sources include fully three-dimensional (3-D) lasers or ion beams using a ray tracing algorithm, temperature sources, frequency-dependent radiation sources, velocity sources, external electric circuits, and pressure sources. Thermonuclear reactions can be modeled by LASNEX, including the energy produced as well as the reaction products and their transport through the problem. We have several different atomic physics packages available which supply the coupling and transport coefficients and self-consistent thermodynamic quantities. LASNEX combines all these physical processes and evolves the system forward in time, rather than just solving for an equilibrium or steady-state configuration. This complexity and the large number of physical processes modeled present a challenge to us (as we try to describe the code) and to those using the code and interpreting the results. A computer simulation of an experiment calculates all the independent physical quantities at each time step to enable the system to evolve forward. Any quantity can be "measured" or monitored. Huge amounts of data are often the problem for computational physicists, rather than a lack of data (which can be a problem for experimentalists).

With LASNEX, a "typical" problem does not exist—its calculations can take many different forms. Because of this, in this paper we describe the code by presenting all its different parts and how they fit together, organized around the "circles and arrows" diagram shown in Fig. 1. Following the descriptions of the physics packages, we outline the computer science enhancements that have been added to increase LASNEX's power, versatility, and convenience. Finally, we present several LASNEX calculations that accurately model laboratory experiments. Ultimately, it is the agreement between the code calculation and experimental data that validates the code and gives us confidence that LASNEX can be used to predict and design future experiments (the National Ignition Facility, for example).

Circles and Arrows Diagram

Figure 1 is a "circles and arrows" diagram that represents the LASNEX computer code: *circles* represent the fields in which energy resides and *arrows* represent the interactions among the various fields. There is also a circle labeled atomic physics that is connected to the arrows. This process supplies the physical data necessary for many of the other packages.

LASNEX solves a large set of coupled, nonlinear, partial differential equations that determine the temporal evolution of the many spatially dependent quantities as they are influenced by different physical processes. The solution of the equations for the different physical processes is "split," so that the code evolves one process after another forward in time by one timestep until they have all been done, feeding the results from one into the next. For each package, a maximum allowable or reasonable timestep is calculated for the next cycle. When all the processes have been solved for one step, the next step is taken using a value for the timestep that is the smallest of all the possible time steps.

One of the basic design philosophies of LASNEX is to allow the different physics packages to be turned on or off by the users based on their particular application. The actual processes that are used in any calculation are determined by the user, usually when the calculation is initialized. Also, in a circle there can be several models for a given physical process. Once again, the physicists will choose which models to use based upon the problem parameters and the computer resources available. This choice of models can also affect the interactions among the different parts of the calculation represented by the arrows. The ability to choose at execute time between alternative modules for the same physical process has allowed us to develop and debug new physics packages while simultaneously maintaining a stable code for production use. Redundant physics models also allow a user to validate the correctness of each model and to trade computer time and problem size for accuracy, according to the needs of the particular situation.

Hydrodynamics

The spatial variation of the physical quantities are described on a 2-D, axially symmetric mesh composed of arbitrarily shaped quadrilaterals. Typically, the hydrodynamics is Lagrangian[5] in which the mesh moves along with the material. LASNEX uses a staggered grid hydro algorithm adapted from the HEMP code of Wilkins.[6] On a regular mesh, it is second-order accurate in time and space. Several artificial viscosities are provided to treat shock waves of arbitrary strength, one of which approximates the dissipation given by a

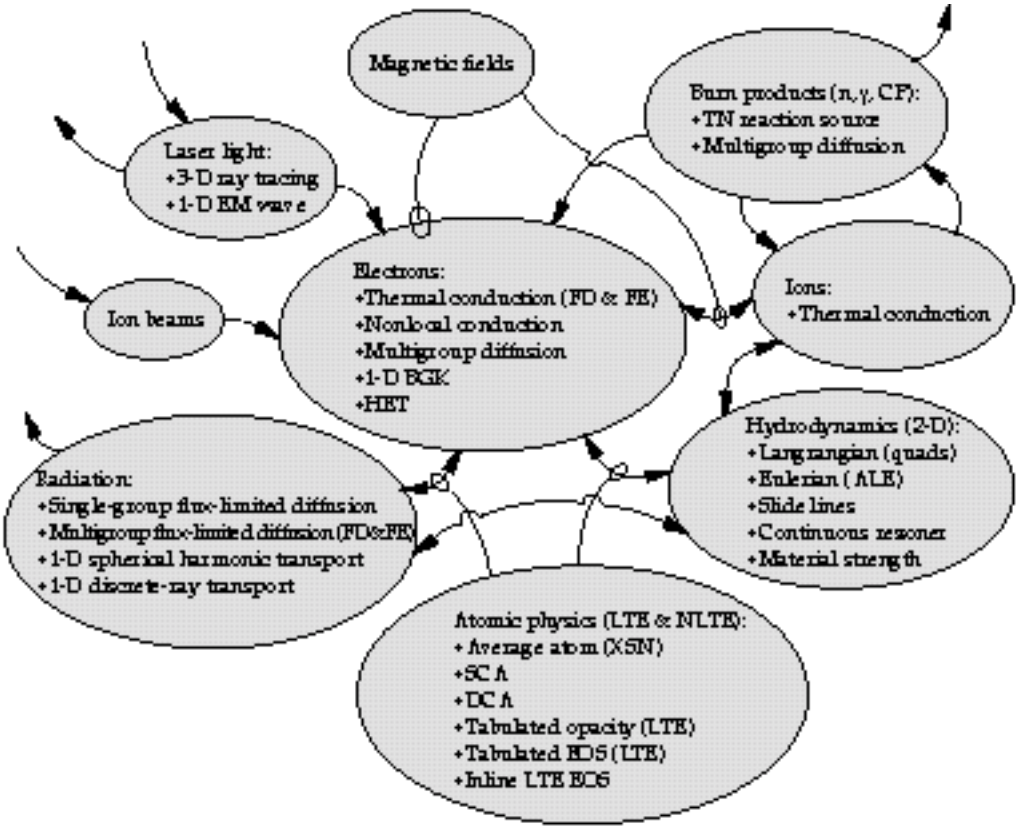

FIGURE 1. A schematic overview of LASNEX. The *circles* represent the fields in which energy resides; the *arrows* represent interactions among the different fields.
(02-08-1292-3795pb02)

Riemann solution of the flow. There are also velocity filters used to damp spurious mesh oscillations, including anti-hourglass filters and artificial shear viscosities.

A material strength capability is available that generalizes the scalar pressure to a stress tensor appropriate for isotropic materials. It includes elastic and plastic flow regimes and a Von Mises yield criterion for the transition to plastic flow. There are provisions for user specification of the elastic constants and yield stress limits to allow very general constitutive models. There is a history-dependent fracture model that includes both compression and tensile failure modes, based on computing a strain damage integral from the plastic flow and using this damage to lower the yield strength in a prescribed way. The model allows effects such as spallation of brittle material to be treated. Its parameters are designed for great flexibility in treating material failure.

The hydrodynamics calculation usually takes a small fraction of the computer time required for a complete physics cycle, and often the Courant timestep (set by the requirement that a signal can travel only one zone width in one timestep) can be much smaller than all the other timesteps. In this case, LASNEX can "subcycle" the hydrodynamics, taking many hydrodynamics cycles per major physics cycle to speed up the calculation.

When the LASNEX hydrodynamics method leads to severe mesh distortions or suboptimal resolution of the important physics, the user can request that the mesh be moved. There are two rezoners used in LASNEX—one for rezones at discrete times and another which operates continuously. The discrete time rezoner takes explicit user input to generate the new mesh coordinates. Discrete rezoning can be done interactively with graphical feedback or can be preprogrammed using Basis[4] interpreted user-defined functions to determine when and how to rezone the problem. (See the "User Interface" section for an example.) The continuous rezoner accepts user commands to define the desired mesh configuration and tries to satisfy these requirements through a relaxation process (one of which tends toward a mesh of equipotential lines). Rezoning every timestep can be equivalent to performing Eulerian or Arbitrary Lagrange Eulerian (ALE)[7] hydrodynamics. It requires that the remapping of all variables to the new mesh be done with high accuracy.

Both of the rezoners use a Van Leer slope limiting method in which spatial quantities are represented as

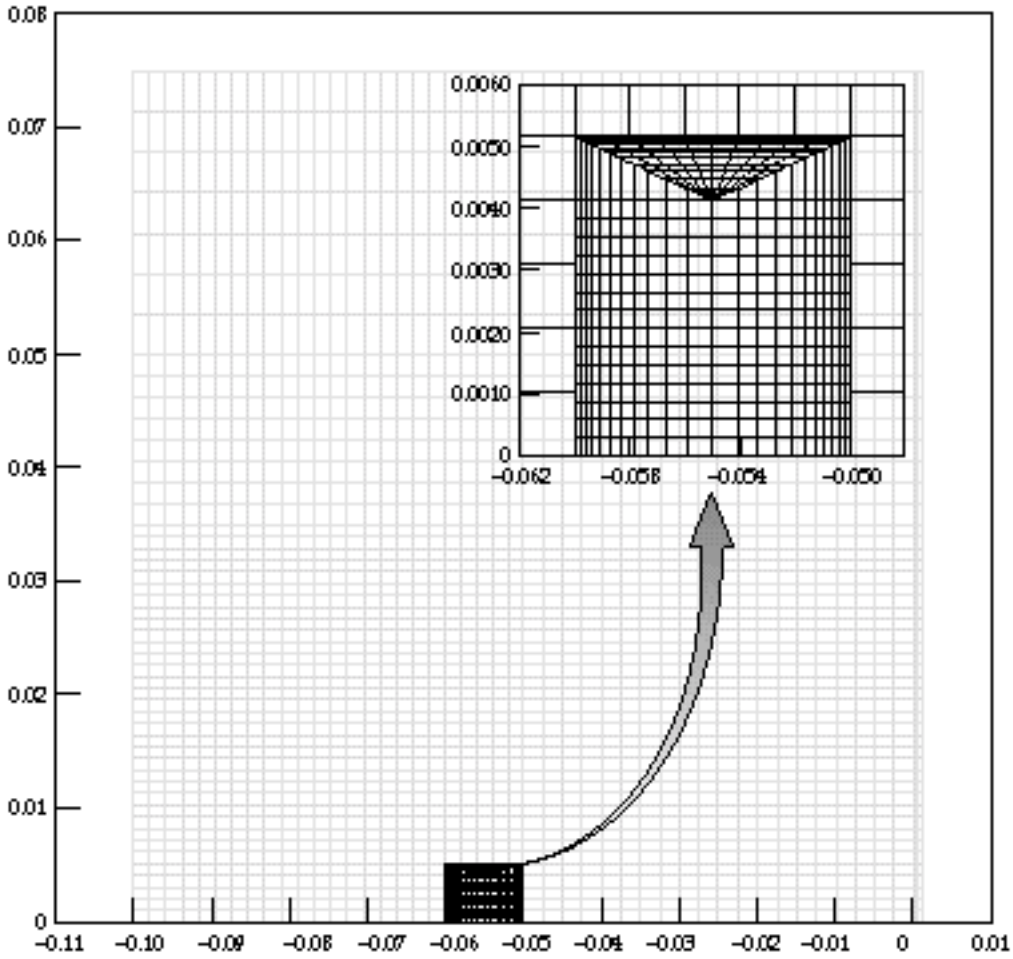

FIGURE 2. This mesh models a small, dense impurity in an otherwise homogeneous, lower density region. It is composed of two simply connected parts that are joined by slide lines. The slide lines allow part of the mesh to be much more finely resolved than the rest of the problem. Without slide lines, the fine zones would have extended all the way in both directions, increasing the problem size by over 50% and creating many small low-density zones with a much more restrictive Courant condition. (40-00-1196-2729pb01)

linear functions within each zone. This allows for second-order remap accuracy in smooth regions, while not generating extraneous maxima/minima at discontinuities. This is adequate for most quantities, but the material composition suffers some numerical diffusion. The addition of a material interface tracking algorithm would substantially reduce these errors.

The discrete rezoner allows an arbitrary overlap between the old and new mesh, but the continuous rezoner demands local overlap of the two meshes. The locality assumption permits an accurate momentum remap that also conserves kinetic energy,[8] while the more general case is treated by a less accurate interpolation method.

Ordinarily, the LASNEX mesh has a simple logical structure in which each interior quadrilateral zone has four nearest neighbors, a relationship that remains constant throughout the calculation. Optionally, one can specify slide lines,[9] logical line segments along which zones on one side are free to slide relative to the other side. This allows simulations with discontinuous velocities and also provides a means of zoning complicated initial geometries, such as shine shields or connecting regions of differing resolution. Figure 2 shows a LASNEX mesh with slide lines to connect regions of differing resolution. Every physics model that involves neighbor zones (hydrodynamics, diffusion, transport, laser ray trace, etc.) has had to be modified to include the special (time-dependent) slide line connectivities. These slide line modifications which connect logically disjoint zones have also been used to establish the periodic boundary conditions needed for multimode *z*-pinch calculations.

Electrons

To model the electrons, the user can choose thermal conduction, multigroup diffusion, one-dimensional (1-D) or 2-D nonlocal conduction, 1-D Bhatnagar, Gross, Krook (BGK) conduction, or a hybrid electron transport (HET) model that is currently under development. All the 1-D models allow either planar or spherical configurations.

Thermal electrons are assumed to be in a Maxwellian distribution. The electron thermal energy is transported using tensorial plasma conductivities in a magnetic field modified by applying a flux limiter (described later). The electrical conductivities in LASNEX go beyond the low-density, high-temperature formulae of Spitzer/Braginskii[10] by including dense plasma effects.[11] They include the effects of electron degeneracy, Debye–Hückel screening, ion–ion coupling, and electron-neutral scattering (see refs. in Ref. 11). The treatment is based on a relaxation time (Krook[12]) model of the Boltzmann equation ignoring e–e collisions. LASNEX approximately includes e–e collisional effects by making Braginskii's correction to the Lee/More coefficients. The cross sections used are analytic fits of a Coulomb cross-section form to numerical partial-wave expansions, with cut-off parameters to avoid unphysical answers. The effects of ion correlations in the liquid/solid regimes are treated by a modified Bloch–Grüneisen[13] formula. Finally, the various magnetic coefficients (which do satisfy the Onsager symmetry relations) are fits to the numerical integrals in the weak-field case and tabulated for the intermediate and strong-field case. Overall, the conductivities are believed accurate to a factor of 2 over a very wide range of densities (to 100× solid) and temperatures (eVs to 100 keV) and expressed in a computationally simple form.

Thermal electron conduction involves the solution of the diffusion equation on the arbitrary quadrilateral mesh. Since the mesh lines are not necessarily orthogonal, this requires a nine-point diffusion operator. The resulting matrix is solved by the Incomplete Cholesky–Conjugate Gradient (ICCG) method.[14] Both a finite difference and a finite element scheme are available to calculate the electron conduction. Finite difference schemes[15] are employed throughout the code to diffuse the zonal quantities, which are the basic unknowns. The finite element method[16] gives better solutions on nonorthogonal meshes. However, the finite element energy densities are point centered and must be integrated into the LASNEX architecture of zonally averaged quantities.

The diffusion equation is derived in the limit of near isotropy. Thus the mean free path should be considerably shorter than the characteristic length scale of the problem. Nevertheless, the diffusion equation can give meaningful results in other regimes if modified to insure that physical expectations will not be violated. The flux of energy should be bounded by the limit of all the energy flowing in one direction at the average velocity of the Maxwellian distribution. This is referred to as "flux limiting" and is achieved by modifying the diffusion coefficient so that when the gradients are very large the energy flux will be bounded by this criterion.

The thermal electron energy is coupled with the other fields in LASNEX as indicated by the arrows in Fig. 1. The energy of the electrons is shared with the ions through Coulomb collisions.[17] The electrons affect the material hydrodynamic motion by contributing to the plasma pressure.

Nonthermal, actually suprathermal, electron distributions can also be treated in LASNEX. This method was developed to study the hot electrons that are found in ICF applications.[18] In the code hot electrons are created by either a laser source or an ad hoc source defined by the user. They are transported and thermalized by a multigroup, flux limited diffusion method that is relativistically correct and allows for arbitrary isotropic distributions.[19] When suprathermal electrons

are being modeled, the thermal electrons are also present. Suprathermal electron transport is iterated, along with the determination of a self-consistent electrostatic potential, in a way that assures zero net current. Suprathermal electrons lose energy to the thermal electrons by Coulomb collisions, including the effect of the degree of ionization[20] and by doing Ohmic work through the electric field. The suprathermal electron bins can have arbitrary bin structure.[21] Suprathermal electron bremsstrahlung is modeled by a parametrized fit to the bremsstrahlung spectrum,[22] which accounts for partial ionization. The suprathermal electrons produce frequency-dependent bremsstrahlung photons that are transported in LASNEX's radiation package. The suprathermals also contribute to the plasma pressure.

The nonlocal electron conduction package in LASNEX solves the electron conduction equation with a nonlocal heat flux that vanishes at the boundaries. This nonlocal package models the features of fully kinetic Fokker–Planck calculations. These features are a reduced heat flux in the hotter region of the heat front, a preheat foot, and nonisothermal, low-density corona.[23] The nonlocal electron transport option is available in both one and two dimensions. The 1-D model solves finite difference equations. (For all 1-D models, LASNEX allows either spherical or planar configurations.) The 2-D nonlocal conduction uses the finite element machinery.

Often in laser-produced plasmas, the range of the hot electrons is much larger than the temperature or density scale lengths, which give rise to free streaming and nonlinearities in the heat conduction. The 1-D BGK[24] electron thermal conduction model accounts for free streaming effects in steep temperature gradients by evaluating the electron distribution within the plasma via the BGK approximation to the Fokker–Planck equation. The resulting distribution is then used to evaluate the heat flux in the plasma.[25] A distribution function approach was developed because other models were unable to account reliably for the nonlocal electron heat transport.[26] The BGK approximation is used to improve the speed of the algorithm over a direct solve of the Fokker–Planck equation. Nevertheless, iteration of the algorithm is necessary to calculate the electric field, insuring charge neutrality and particle and energy conservation, neither of which is explicitly guaranteed by a blind application of the BGK approximation.

A package for hybrid electron transport (HET) is being developed to incorporate 2-D electromagnetic effects into electron transport. The model draws heavily on the ideas of Rodney Mason, associated with 2-D implicit plasma simulations.[27] The algorithm is designed to incorporate particle and/or fluid electrons—the particles would represent hot electrons generated by plasma processes, and the fluid electrons would represent the background thermal electrons. Currently, only the field solver and the thermal electron parts of the package are implemented. The package accounts for electron transport via a generalized Ohm's law[28] which includes all of the Braginskii coefficients,[29] including the Hall and Nernst terms. For heat transport, the package also includes all of the Braginskii coefficients, including the Righi–Leduc term. Because the electric field is also important in transport, a field solver for Maxwell's equations, including the displacement current, was written that goes beyond the MHD approximation used in the present magnetic field package in LASNEX.[30] The MHD approximation assumes charge neutrality in the plasma which results in the displacement current being ignored. The HET package does not ignore the displacement current and therefore is not charge neutral. HET also does not ignore $\partial j/\partial t$. The fields are represented by continuous finite elements; the electric current is represented by discontinuous finite elements. The effects on transport using this model are already dramatic. In some situations the spontaneously generated magnetic field magnetizes the electrons with the result that thermal transport is inhibited. Improved results for laser-heated foil experiments have been noted.[31]

Ions

Thermal ions are assumed to be in a Maxwellian distribution. Flux limited diffusion methods are used to mix spatially different types of ions and to transport the ion thermal energy. Ion conduction uses the same ICCG method to solve the diffusion matrix as the electron conduction package. Real ion viscosity (momentum diffusion) is optionally included in the hydrodynamics equations, although it is typically small by comparison with the usual artificial viscosity.

The ions affect the material hydrodynamic motion by contributing to the pressure. Hydrodynamic work, including that done by the artificial viscosity, and the thermonuclear reactions heat the ions. The heat exchange with the electrons limits the ion temperature. The ion temperature is important for three practical reasons: (1) the thermonuclear fusion reaction rate is very sensitive to T_i; (2) T_i controls the Coulomb logarithm used to calculate laser absorption by inverse bremsstrahlung and electron thermal and electrical conduction; and (3) T_i determines the Doppler contributions to the width of spectral lines, which can be important for x-ray laser designs.

Radiation

Radiative energy flow is one of the principal means of coupling laser energy into a target. Because of its importance in ICF, LASNEX has several methods

for calculating radiation transport: single group flux limited diffusion, multigroup flux limited diffusion using either finite difference or finite element solution scheme, 1-D spherical harmonic expansion of the transport equation, 1-D discrete-ray transport, and detailed radiation transport.

Single group flux limited diffusion assumes that the photons are in a Planck distribution characterized by a local radiation temperature. This method uses only Rosseland mean opacities and is valid if the system is thick to radiation.

Multigroup flux limited radiation diffusion assumes nearly isotropic photon distributions and allows for arbitrary frequency dependence. Frequency-dependent opacity data is required. The diffusion algorithm to model multigroup radiation diffusion can be treated by either the finite difference approximation or the finite element method,[32] similar to the electron diffusion. The ICCG linear system solver is employed in both schemes. By default, the finite difference and finite element models use an iterative scheme to couple the radiation energy to the matter.[33] A "partial temperature" coupling scheme which is often much faster (see Ref. 42) is also available for use, but it can give large swings of the intermediate values of the electron temperature during a single timestep, decreasing accuracy. Accuracy is controlled by reducing the timestep until the swings in the partial temperature are acceptable. However, this can result in very small timesteps. The recommended radiation electron coupling scheme is differenced implicitly in time; in steady state, it will relax to the correct answer in one step. This method, related to a scheme of Axelrod and Dubois,[34] may be thought of as a form of alternating-direction implicit iteration, in which one direction corresponds to photon energy and the other to spatial location. In certain circumstances, particularly when the timestep is large and the rates associated with transport and radiation-matter coupling are similar, the convergence can be quite slow. We have a convergence-acceleration scheme for use in these unusually stiff cases.[35] Shestakov et al.[36] describe test problems in radiative transfer and compare finite difference and finite element solutions to the radiation diffusion equations, illustrating the use of analytic solutions to validate the results of computer simulations.

Photon Compton scattering and its resulting energy exchange with electrons is also treated in LASNEX. To model relativistic Compton scattering, we evaluate the Compton scattering kernel by averaging the Klein–Nishina cross section over a relativistic Maxwellian distribution.[37] This scattering kernel is then integrated over all directions to obtain the transfer matrix used to solve the Boltzmann equation for isotropic photon distributions.[38] Finally, one can make the Fokker–Planck approximation which assumes that the photon frequency shift is small compared with the photon frequency.[39] LASNEX can do Compton energy exchange by either the Boltzmann or Fokker–Planck methods. The Fokker–Planck method is finite differenced in a way that obtains exact steady-state results.[40] Since x-ray mean free paths are often comparable to the size of ICF targets, the diffusion approximation is not appropiate and we must solve the transport equation.

LASNEX has a 1-D (either spherical or slab) P_n radiation transport package in which the photon angular distribution is expanded in spherical harmonics where P_l is the coefficient of the lth Legendre polynomial.[41] The radiation transport equation is written as an infinite set of coupled equations for the P_l's. Rather than terminating this infinite set at the lth moment by zeroing out P_{l+1}, Kershaw improved the results of the P_n calculation by setting P_{l+1} to a value within its bounds. Probability theory is used to calculate the upper and lower bounds. The 1-D P_n package uses the same relativistic Compton methods described earlier to evolve the 0th (isotropic) moment. Other moments only undergo Thompson scattering with no frequency shift. The P_n package couples the photon energy to matter using the "partial temperature scheme."[42] The 1-D P_n radiation transport has been useful both in actual design calculations and in testing the accuracy of various extensions to the diffusion theory.

Radiation transport in LASNEX is also modeled by a 1-D discrete-ray method.[43] It consists of solving the finite difference equations for the radiation intensity for a few selected directions. The total intensity at any point in space is the sum over the intensities of each of the discrete directions weighted in some consistent way, for example, by the fraction of the solid angle that each ray represents. We difference the radiation transport equation using upstream, implicit differencing, and we couple the radiation energy with matter by iteration using the multifrequency gray approximation.[44] A persistent problem with the Lund–Wilson scheme has been the accuracy in the thermal wave limit, when the zones are many mean free paths thick. LASNEX also has a 1-D, discontinuous finite element radiation transport package, bilinear in space and photon direction, which behaves correctly in the thermal wave limit.[45] The radiation transport equation has upwinded, discontinuous elements; the electron temperature equation has continuous elements. The resulting linear equations are solved by a modified splitting of the intensity and temperature parts. There is an optional Newton iteration for problems where the nonlinearity of the Planckian function is significant over a single timestep. In this, the Compton scattering is treated nonrelativistically, including scattering only in angle (Thomson scattering).

All radiation transport models deposit momentum when a photon is absorbed or scattered. In the Atomic Physics section, we describe the derivation of the

frequency-dependent radiative opacities used in the photon transport packages. Basically, we include bound-bound, bound-free, and free-free processes in either local thermodynamic equilibrium (LTE) or non-LTE. The frequency-dependent radiation intensity that escapes from a LASNEX mesh is often a very valuable problem diagnostic to compare with corresponding experimental spectra.

Lasers, Ion Beams, and Other Sources

A LASNEX calculation can be driven by several different types of sources and/or boundary conditions. Some sources, such as temperature, pressure, frequency-dependent radiation intensity, and velocity are imposed arbitrarily, while the beam deposition sources interact with the plasma in a more complete and physically consistent manner. Lasers and ion beams are calculated by tracking a number of rays through the spatial mesh. Power on the ray is decremented as deposition occurs. The temporal and spatial variations of all the possible sources can be specified by the users.

In 1983, a 3-D laser ray tracing package was added to LASNEX.[46] Prior to this, all light rays were forced to travel in the *(r,z)* plane, which often created anomalously high intensities near the symmetry axis. The 3-D laser package computes the trajectories of an arbitrary set of laser rays through the mesh. The rays are bent according to the laws of refraction. Ray trajectories are computed using the gradient-index geometrical-optics equations. On the basis of computed ray path lengths, energy is deposited in each zone by inverse bremsstrahlung, including nonlinear corrections.[47] The laser energy is also absorbed by a photoionization model based on the Saha equation.[48]

Noncollisional processes—plasma instabilities and resonance absorption—are modeled by angle-dependent absorption[49] or more simply by absorbing a given fraction of the energy that is left in each ray at its turning point. The ray intensity is correspondingly attenuated. When suprathermal electrons are present, absorption by the noncollisional process creates an electron distribution with a "hot" temperature derived from fits to plasma simulations.[50]

Typically, the LASNEX computational mesh is too course to resolve steep, inhomogeneous plasma-density structures that might arise from uneven illumination or hydrodynamic instabilities. Therefore, the code has a statistical model of the refractive scattering of laser light by random density fluctuations in the subcritical plasma.[51] The scattering can occur along the entire ray path or only at the turning point. The hydrodynamic effect of the laser light is included with a ponderomotive force algorithm which has both scalar and tensor terms.[52]

Since LASNEX tracks a finite number of rays through the mesh, we often see "ray effects," causing the laser intensity to vary unphysically. A "fatray" package smoothes the laser energy deposition, using a finite element diffusion equation.[53] This will not cause energy to be deposited past the critical surface because the smoothing takes place only for regions where the electron density is less than or equal to the critical electron density. Another option to decrease the ray effects (which we call "smearing") is to average the deposition over two zones each time it is applied, and it can be applied any number of times. The user has some directional control by choosing to apply the smearing along particular logical mesh lines.

Charged-particle beam deposition is calculated from stopping-power formulas that account for straggling and partial ionization.[54] We have made calculations from first principles of the dynamic charge state of a fast, heavy ion as it experiences various ionization and recombination processes while slowing down in a heated target material.[55] The important processes are collisional ionization balanced at equilibrium by radiative recombination.

Ion beams do not refract as light does. Therefore, we have a separate, simpler and faster ray trace package for ions. It assumes only straight ray paths in 3-D, which become hyperbolae when projected onto the (r, z) plane.[56] Momentum deposition from ion beams is implemented consistently.

For moderately intense, ultrashort pulse lasers, we have a subroutine which actually solves Maxwell's equations in 1-D, rather than using a ray trace approximation.[57] The algorithm takes advantage of the rapid oscillation and propagation of light waves compared with hydrodynamic motion. Thus, the steady-state 1-D solution to Maxwell's equations results in the Helmholtz equations. Both *s*- and *p*-polarized cases are accounted for by the package. Plasma waves are generated at the critical surface in the case of *p*-polarized light. To account for losses due to plasma waves without explicitly following the waves in the plasma, the total collision rate is modified in the resonance region to be the sum of: the electron–ion collision rate + the Landau damping rate at the critical point + the rate at which plasma waves leave the resonance region + the loss rate due to the wavebreaking of the plasma waves.[57] To maintain consistency, the algorithm automatically incorporates a WKB approximation in the low-density blow-off region when the low-density zone sizes approach the laser wavelength. The frequency-dependent conductivity has been improved to go beyond the Drude approximation and results in improved modeling of absorption in solids.

Burn Products

LASNEX calculates all significant thermonuclear reactions among isotopes of H, He, Li, Be, and B.[58]

Charged particles and neutrons produced are transported by multigroup diffusion methods that take into account nuclear scattering, in-flight reactions, and momentum deposition.[59] Gamma rays produced by inelastic nuclear interactions are also transported by multigroup diffusion, accounting for Compton scattering, photoionization, and pair production.[60] The neutron and gamma diffusion both use a multigroup extension of Levermore's diffusion method.[61] The charged particle transport is an extension of diffusion that retains particle inertia as it undergoes straight-line energy loss to electrons.[62] Charged particle energy loss rates include the effects of an arbitrary ratio of particle to electron thermal velocity, Fermi degenerate electrons, and bound electrons.[63] All burn products either escape from the problem, providing numerous diagnostic opportunities, or deposit their energy back into the thermal electron and ion fields.

Magnetic Fields

Magnetic fields are generated automatically in 2-D problems or can be imposed by user-specified sources. The magnetic field package[64] in LASNEX includes J × B forces and the full Braginskii cross-field transport model. The Braginskii model has been extended with the Lee and More conductivities and includes the magnetic diffusion, Nernst, grad P, grad T, and Hall terms in Ohm's law, as well as the perpendicular and Righi–Leduc heat flows, j•E, and other terms in the heat equation. The user may optionally specify source terms that self-consistently couple the plasma to an external LRC circuit.

If requested, the magnetic package modifies the electrical conductivity to account for the anomalous resistivity due to lower-hybrid waves. Periodic boundary conditions are available for the study of multimode Rayleigh–Taylor (RT) perturbations. The energy conservation has been improved (order-of-magnitude improvement for 1-D, purely-Lagrangian calculations) and the magnetic flux is conserved during mesh rezoning. These enhancements, together with new, high-resolution rezoning schemes, programmed by the users with the Basis interface, have allowed the successful modeling of high-energy, radiating *z*-pinches. Features typically exhibited in these simulations are the strong nonlinear growth of magnetic RT modes,[65] and the formation of hot spots[66] near the axis due to unstable ($m = 0$) sausage modes.

Also, magnetic fields can be spontaneously generated in the presence of nonparallel temperature and density gradients which may occur in laser-produced plasmas. The resulting changes in the magnetic-field-dependent transport coefficients for all charged particles may significantly alter the plasma temperature and pressure profiles. This may be an important effect in the design of some hohlraums or direct-drive targets which require a high degree of symmetry and efficient utilization of laser power.

Atomic Physics

The atomic physics models in LASNEX supply the equation-of-state (EOS) variables (e.g., pressure and energy as a function of temperature and density) used in the hydrodynamics, the degree of ionization used to establish various electron collisional rates, and the frequency-dependent opacities used by the radiation transport routines. In LTE, these quantities are functions only of the density and electron temperature and can be conveniently tabulated or evaluated by analytic expressions. LASNEX can access the internal Lawrence Livermore National Laboratory (LLNL) EOS data and the Los Alamos National Laboratory (LANL) Sesame data,[67] and it can use its own quotidian EOS (QEOS) package.

The QEOS[68] is an in-line EOS routine that is based on the Thomas–Fermi electron-gas approximation. The QEOS total energy is split up into three parts:

$$E_{\mathrm{tot}}(\rho, T) = E_{\mathrm{e}}(\rho, T) + E_{\mathrm{b}}(\rho) + E_{\mathrm{n}}(\rho, T) \qquad (1)$$

where E_{e} is the Thomas–Fermi (TF) energy, E_{b} is an analytic (Cowan) bonding correction used to fit the experimentally known solid density and bulk modulus at standard temperature and pressure, and E_{n} is the nuclear motion energy. It provides separate EOSs for electrons and ions. Since QEOS is based on a free energy, thermodynamic consistency is guaranteed, and the smooth TF term together with the analytic ion part generate continuous results from cold solid conditions through the liquid, vapor, and plasma states. The *Z*-scaling property of the TF model allows a single table to generate data for any element as well as provide the speed necessary for an in-line calculation.

LASNEX can also access LTE frequency-dependent opacity data in three different formats: it reads Cray binary files of opacity information in a format unique to LASNEX designed 20 years ago; it reads the LANL Paradise[69] opacity files; and it reads the LLNL machine independent opacity files,[70] using the portable data file (PDB) library of Stewart Brown.[71]

In non-LTE, the EOS, degree of ionization, and the opacity must be determined from the atomic populations which are found by solving rate equations and, in general, depend on the photon and suprathermal electron distribution functions. LASNEX has incorporated three major atomic physics packages, XSN, SCA, and DCA, which can be run in either LTE or non-LTE modes. All three provide LASNEX with pressure, energy, and frequency-dependent opacity and emissivity due to bound-bound, bound-free, and free-free processes.

XSN[72] is an average atom, atomic physics code that uses a simple *Z*-scaled, screened hydrogenic model to perform in-line calculations of arbitrary mixtures at all temperatures and densities. It is used to obtain material opacities for LTE and non-LTE, as well as EOS values under non-LTE conditions. It includes the effects of Fermi degeneracy, continuum lowering, and pressure ionization,[73] which are required to correctly model cold solids at high densities and is designed to closely match the Thomas–Fermi ionization values along the cold curve. The lack of *l*-splitting and the simple line-width formulae limit the accuracy of the opacities to average values. However, XSN's simplicity does provide the required speed and allows any mixture to be treated. Since the EOS is based on a free energy, it is automatically thermodynamically consistent. The lack of a bonding correction means that XSN's pressures at low temperature are too high, but in most cases, non-LTE effects are small under those conditions, and this package would rarely be run.

The average-atom atomic physics package Statistical Configuration Accounting (SCA)[74] produces more accurate opacity information than the default XSN package because its underlying atomic physics data is evaluated off line by a self-consistent, relativistic, Hartree–Slater program, called LIMBO.[75] Because the database which LIMBO produces is based on relativistic physics, the resulting opacity which SCA produces shows fine-structure splitting. Whereas, fine-structure splitting can be included into an XSN opacity only in an ad hoc fashion. As in XSN, the atomic physics is simplified by using the hydrogenic approximation, where the states of an ion are described by the quantum numbers of a single electron which is immersed in a spherically symmetric screened Coulomb potential.

The Detailed Configuration Accounting (DCA) atomic physics package[76] solves rate equations for the number of ions in each important excited state in each ionization state. This package is more expensive than XSN or SCA. It is used when accurate atomic physics is needed for line diagnostics or x-ray laser modeling. DCA can handle any number of states connected by radiative and collisional bound-bound, bound-free, and auto-ionization and dielectronic recombination processes. The states and transition rates are specified in data files generated by other codes. Optionally, a simple screened hydrogenic model can be produced at problem initialization. In addition, the DCA package calculates Voigt line shapes due to Doppler, Lorentz, and Stark broadening and, if requested, handles line transfer by a general purpose escape probability method that reduces to 1-D, static or Sobolev limits in planar or cylindrical geometry.[77] It includes effects of Fermi degeneracy and handles pressure ionization and continuum lowering in the Stuart/Pyatt approximation[78] by reducing the statistical weight smoothly to zero as continuum lowering ionizes the weakest bound electron. To save computer time, the levels which are eliminated by continuum lowering or which are ionization states of low probability are removed from rate calculations and from the system of rate equations. The resulting reduced linearized system is then solved by banded or iterative matrix methods.

Another relatively new feature of the LASNEX atomic physics package is a multiphoton, dielectric breakdown package which models multiphoton–ionization seeding of avalanche breakdown. The model is based on the work of Feit et al.[79] in which a simple seeded exponential model was inferred from their Fokker–Planck studies. The seed rate is proportional to an integral power of the energy density of the laser light in the material. In this process, the electron density will build until a threshold level is reached. Above the threshold, the material breaks down by electron avalanche, which is modeled by an electron distribution that exponentially increases in time. The avalanche is quenched when a maximum of one electron per ion is reached, justified by assuming that the ionization potential for the next electron to be removed increases substantially.

User Interface

LASNEX has been a pioneer in interactive and steered computations. Even in its early days (more than twenty years ago), the users were able to investigate and modify their simulations while they were running. Graphical displays and numerical edits of the problem could be produced at any time, allowing the users to ascertain quickly whether the problem was running correctly and efficiently. With the inclusion of the Basis code development system,[80] a huge leap in interactivity was achieved at once. The programmable interface provided by Basis transformed LASNEX into "a whole new generation of design code."[81] It gives LASNEX a complete, up-to-date, well maintained, and well documented computer science interface, allowing users to innovate without the intervention of the code developers. The code developers no longer have to get involved with specific user requests for diagnostics or special purpose models, freeing them from straightforward but time-consuming tasks.

Basis has a fully featured, FORTRAN-like interactive programming language interpreter which can access the variables and functions in the LASNEX compiled code. Basis supplies an interface to a complete graphics package that includes curves, markers, contours, text, frame control, and viewport control, as well as LASNEX-specific plotting commands, such as mesh plots and mesh-based contour commands. Basis also offers many mathematical packages, such as Bessel functions, fast-Fourier transforms, random-number generators, and polynomial fitting.

One of the most important components of Basis is a history package that allows the user periodically to execute specified commands and/or to collect any number of sets of values of arbitrary expressions. A variety of mechanisms can be used to select the frequency at which these generations are collected. Users may also specify logical conditions under which actions will occur, such as the occurrence of bowties, a zone reaching a certain temperature, etc. The history package employs the portable database system (PDB)[71] to store the collected data. The Portable-Files-from-Basis (PFB) package of Basis gives the users a convenient interface to the data files.

LASNEX users now accomplish many tasks using the tools of the Basis system. They have automated the tedious chore of generating sets of similar problems by writing Basis functions to do the work. Instead of a user issuing instructions from the terminal for a discrete problem rezone, they now can use the Basis interpreter and history functionality to sense when the mesh is in trouble, decide what should be done, and execute the rezone. In this way, LASNEX provides user-controlled, automatic mesh refinement facilities.

In many processes the users can add their own models to work with or to replace those of LASNEX. To accommodate the users' new programming power, we have introduced many "user defined arrays," in which they calculate their own values for various LASNEX quantities. For example, a user can supply the material EOS by calculating, at each timestep, the electron pressure and its derivatives with respect to density and temperature, the electron energy and its derivatives, and the corresponding ion components. Similarly, a user can define the thermal conductivities, zonal energy sources, zonal energy leak rates, or zonal electron thermal flux limit multipliers. We continue to add more user-defined variables to the code to take advantage of this capability.

Another application of the Basis interpreter is to create self-tuning simulations or a self-optimizing series of simulations. As a calculation is running, the Basis interpreter can decide how well the design is working based on certain criteria. Then, for example, the laser pulse shape or spatial profile can be changed to satisfy the criteria better.

Table 1 provides an automatic rezoning example to illustrate how Basis works within LASNEX to save the designers' time and to allow many jobs to run to completion without user intervention.

TABLE 1. Example of automatic rezoning.

Problem Description:

Whenever any zone becomes folded over on itself ("bowtied"), return the mesh to a given "good" configuration, perform the rezone (mesh overlay and remapping of all the LASNEX variables), and proceed.

The user must define the function that tests the LASNEX mesh for troubles (here bowties) and corrects it, if necessary. In this example the mesh is simply set back to the original configuration defined when r_good and z_good were declared. The "h" card tells when (i.e., at every cycle from 1 to 10000) the function, "test_n_rezone," should be invoked.

Note: the "#" symbol indicates that the following text is a comment.

The Basis Coding:

```
real8 r_good = rt, z_good = zt   # Declare "good" coordinates and
                                 # equate to LASNEX's rt and zt.
h 1:10000:1 test_n_rezone        # At every cycle call the function
                                 # test_n_rezone.
function test_n_rezone           # Function definition.
  if(nbowt(rt,zt,ireg).ne.0) then # Test for bowties.
    prezone                      # Execute LASNEX command to
                                 # prepare for rezoning.
    rt=r_good                    # Reset the LASNEX mesh to the
    zt=z_good                    #"good" ones.
    rezone                       # Mesh overlay and remap physical
                                 # quantities.
  endif
endf
```

Example Calculations

This section describes three ICF experiments simulated with LASNEX: a planar hydrodynamic instability experiment, a spherical hydrodynamic instability experiment, and a capsule implosion mix experiment. These examples illustrate that LASNEX can accurately model actual laboratory experiments.

Planar Hydrodynamic Instability Experiment

A series of experiments was conducted with the Nova laser to measure hydrodynamic instabilities in planar foils accelerated by x-ray ablation.[82] We show results of a single-mode experiment and the corresponding LASNEX calculation. A low-density fluid pushing on a high-density fluid is RT[83] unstable, and perturbations on the surface between the fluids grow and take on a characteristic bubble and spike appearance. In these experiments, surface perturbations were imposed on one side of a foil that was mounted across a diagnostic hole in the wall of a cylindrical Au hohlraum. The foil was accelerated by the indirect x-ray drive generated by focusing eight pulse-shaped Nova beams into the hohlraum and was backlit with a large area spot of x-rays created by shining another Nova beam on discs of Mo, Rh, Sc, or Fe. Figure 3(a) shows the experimental image of a foil with 100-μm sinusoidal perturbations viewed side-on with a 2-D grated x-ray imager at 4.4 ns into the pulse. The foil has evolved into the classic bubble and spike shape characteristic of nonlinear RT instability. The LASNEX calculation Fig. 3(b) at 4.4 ns agrees with the experimental image. In fact, they are almost identical.

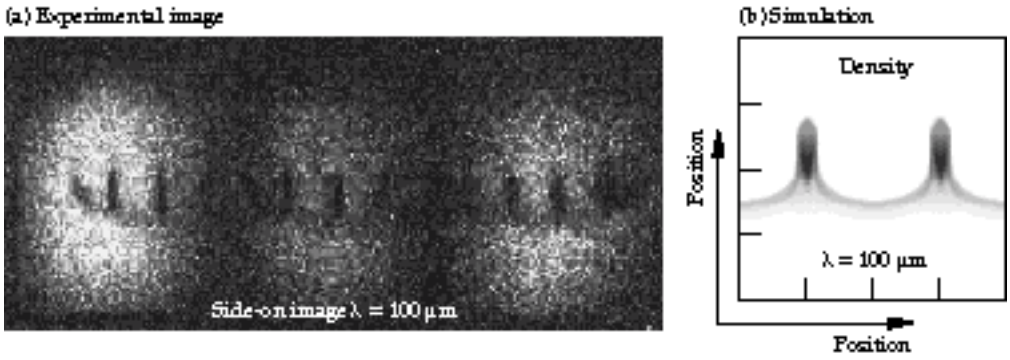

FIGURE 3. (a) Results of perturbation growth experiment viewed side-on at a time of 4.4 ns. (b) Shaded density plot of the transmitted backlighter x-rays at 4.4 ns in the corresponding 2-D LASNEX simulation.
(20-03-1293-4393pb02)

The 2-D LASNEX simulation used the time-dependent laser power that was measured in the experiment, tabular opacities created by a "first principles opacity" code, and tabular EOS data. The transmitted backlighter x-rays included the instrumental response.

Spherical Hydrodynamic Instability Experiment

The next experiment was designed to study the physics of implosions with high RT growth factors. Using indirect drive, we imploded capsules with Germanium-doped ablators to minimize x-ray preheat and shell decompression and hence increased the in-flight aspect ratios. X-ray backlit images of the capsule implosion were recorded at 4.7 keV with 55 ps and 15-μm resolution. Three parallel 3-μm-deep grooves were machined in the ablator to seed the instability. One groove encircled the center of the target; the other two were parallel and on opposite sides. Figure 4 showsthe backlit image of the capsule from the experiment and the LASNEX calculation at 2.22 ns to be virtually identical.[84] The grooves machined into the ablator for this experiment were not uniformly spaced—the one on the right was closer to the center; the effect of this is seen in both the experiment and code results. The groove on the left being farther from the center allowed a double ridge to be created as the perturbation amplitude grew from each groove. This did not occur on the right side, where the grooves were closer and the RT growth from the central and right-hand grooves merged into just one modulation. The LASNEX simulation was a standard 2-D calculation. It was able to accommodate many zones while still properly modeling the radiation by using a special method of weighting opacities that allows a faster convergence with a much smaller number (typically 5 or 6 compared with 50 to 100) of photon groups compared with the standard Rosseland weighted mean.[85]

Capsule Implosion Mix Experiment

This experiment addressed the issue of the hydrodynamic stability of the imploding fuel capsule. Experiments on Nova were performed to study how imperfections on the capsule surface grow by RT instability into large perturbations that cause pusher–fuel mix and degrade the capsule performance.[86] To diagnose

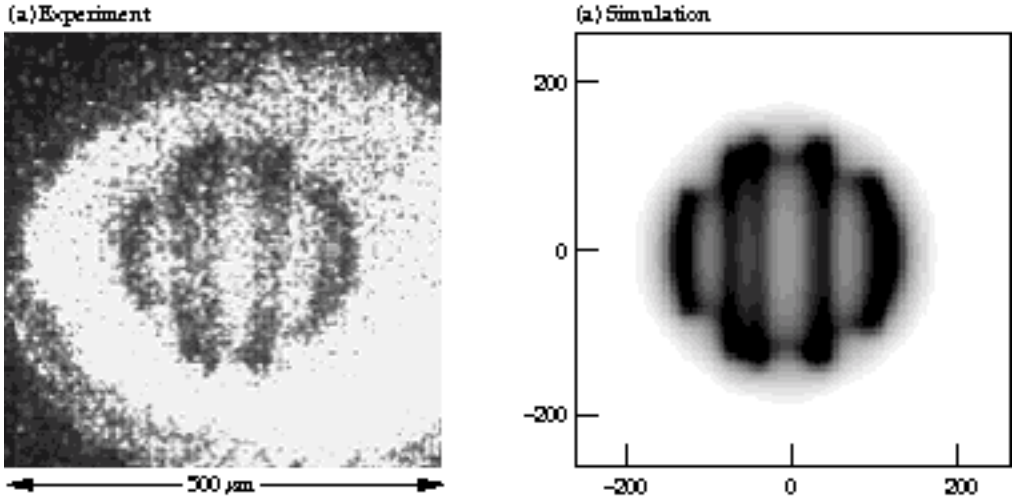

FIGURE 4. Backlit image of grooved Ge-doped imploded capsule at 2.2 ns into the pulse. Both the experimental data on the left and the LASNEX results on the right show the growth of the modulation.
(40-00-1196-2730pb01)

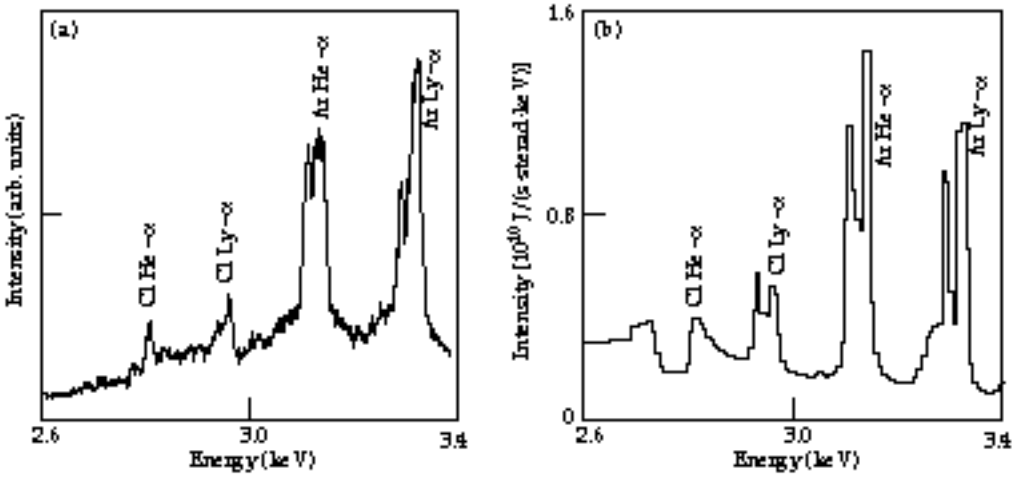

FIGURE 5. Spectra at peak x-ray emission in units of 10^{10} J/s/sterad/keV from the implosion of a smooth surface capsule. (a) The experimental streaked crystal spectrometer data. (b) The 1-D DCA LASNEX simulation result. Relevant emission lines of Cl (the pusher dopant) and Ar (the fuel dopant) are labeled. (20-03-0795-1850pb02)

the enhanced mix, x-ray emission spectra of trace elements in the pusher (Cl) and fuel (Ar) were measured as the surface roughness increased. (Figure 5 shows example spectra.) The emission of the pusher dopant relative to the fuel dopant did increase with surface roughness as the cold pusher mixed more thoroughly with the hot fuel, due presumably to RT instabilities (see Fig. 6). Simulating the implosion of these capsules was a multistep process, employing both 1- and 2-D LASNEX calculations. The 2-D calculations were used to estimate linear growth for single-perturbation modes. The surface roughness and the linear perturbation growth factors combined with Haan's[87] nonlinear saturation prescription were used to calculate the time-dependent width of the mix region. In 1-D implosion simulations with LASNEX, material was atomically mixed and thermal transport enhanced over a distance about the fuel–pusher interface, according to the width of the mix region.

Emission spectra were generated with the DCA atomic physics package. As seen in Fig. 6, the LASNEX results for the ratio of time-integrated Cl to Ar Lyman–alpha emission agrees well with the experimental results. The trend of increased mix for rougher surfaces is very apparent. The experimental spectra and the spectra calculated by LASNEX also match as seen in Fig. 5.

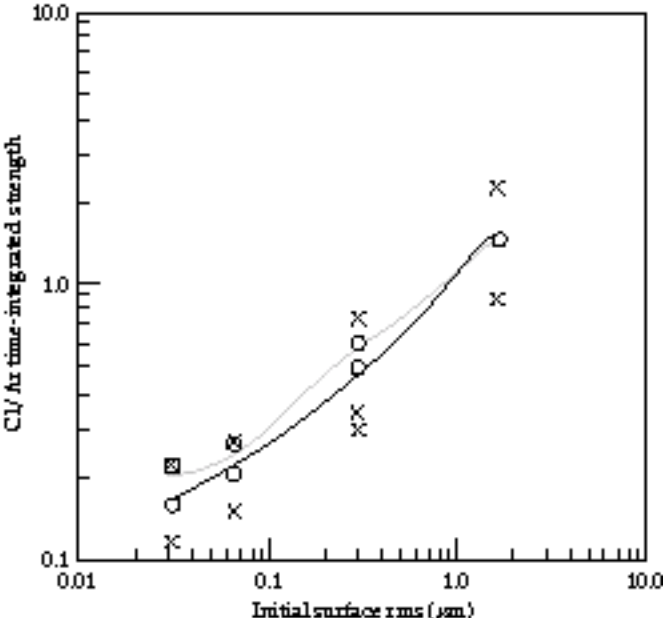

FIGURE 6. The ratio of the time-integrated Cl and Ar Lyman–alpha emission lines is plotted vs the initial surface roughness. An X (O) marks each experimental (simulation) point. The black (gray) lines connect the average values of the experimental (simulated) data at each distinct initial surface rms. (08-00-0996-2154pb01)

Acknowledgments

The extensive references in this article illustrate the number of scientists that have worked on LASNEX. In addition to George Zimmerman who originated LASNEX, we would like to acknowledge all those who have also contributed to it: Roberta Allsman, Harry Bruestle, Lee Busby, Paul Dubois, Art Edwards, Alex Friedman, Fred Fristch, David Kershaw, Jim Kohn, Zane Motteler, Dale Nielsen, Paul Nielsen, Jeff Painter, Manoj Prasad, Rich Sacks, Alek Shestakov, Al Springer, Lynd Stringer, Janet Takemoto, Susan Taylor, Sharon Wilson, and Brian Yang. The support and encouragement of John Nuckolls and Lowell Wood were instrumental in its early development and application. We also acknowledge the continuing support by division leaders from A, CP, and X-Divisions—from Peter Moulthrop and Bill Lokke through Dave Nowak, Dan Patterson, and Mordy Rosen. Feedback from the LASNEX users has also been invaluable, ranging from their encouragement and clever ideas to bug reports and complaints.

Notes and References

1. J. Nuckolls, L. Wood, A. Thiessen, and G. B. Zimmerman, *Nature*, **239**, 5368, pp. 139–142 (1972).
2. G. B. Zimmerman and W. L. Kruer, comments in *Plasma Physics and Controlled Fusion* **2**, 51 (1975).
3. G. B. Zimmerman, *Laser Programs Annual Report*, 3–71, Lawrence Livermore National Laboratory, Livermore, CA, UCRL-50021-80 (1980).
4. P. F. Dubois, "Making Applications Programmable," *Computers in Physics* **8**(1), Jan–Feb 1994.
5. W. Schultz, *Methods in Computational Physics* (Academic Press New York, 1970), vol. 3, p. 1.
6. M. L. Wilkins, *Meth. Comp. Physics* **3**, 211 (1964).
7. F. W. Harlow and A. A. Amsden, *J. Comp. Phys.* **16**, 1 (1974).
8. D. S. Bailey, *Laser Programs Annual Report*, 3–57, Lawrence Livermore National Laboratory, Livermore, CA, UCRL-50021-84 (1984).
9. M. L. Wilkins, "Calculation of Elastic–Plastic Flow" in *Methods in Computational Physics*, Bernie Alder, Sidney Fernbach, and Manuel Rotenberg, Eds. (Academic Press, New York, NY, 1964).
10. S. I. Braginskii, "Transport Processes in a Plasma," in *Reviews of Plasma Physics*, M. A. Leontovich, Ed. (Consultants Bureau, N.Y. 1965), vol. 1, p. 205.
11. Y. T. Lee and R. M. More, *Phys. Fluids* **27**, 1273 (1984); Y. T. Lee, R. M. More, and G. B. Zimmerman, "A New Electron Transport Model for LASNEX," *Laser Programs Annual Report*, 3–61, Lawrence Livermore National Laboratory, Livermore, CA, UCRL-50021-81 (1981).
12. N. A. Krall and A. W. Trivelpiece, *Principles of Plasma Physics* (McGraw–Hill, New York, 1973) p. 317.
13. J. M. Ziman, *Principle of Theory of Solids* (Cambridge University Press, Cambridge, England, 1964).
14. D. S. Kershaw, *J. Comp. Phys.* **26**, (1978); *Ibid*., **38**, 114 (1978); *Idem*, "Solution of Single Tridiagonal Linear Systems and Vectorization of the ICCG Algorithm on the Cray-1," in *Parallel Computations*, (Academic Press, New York, NY, 1982; *Idem*, *Laser Programs Annual Report*, 3–77, 3-79, Lawrence Livermore National Laboratory, Livermore, CA, UCRL-50021-79 (1979); *Ibid*., 3–67, UCRL-50021-81 (1981).
15. G. J. Pert, *J. Comp. Phys.* **42**, 20 (1981); D. S. Kershaw, *Laser Programs Annual Report*, 4–52, Lawrence Livermore National Laboratory, Livermore, CA, UCRL-50021-76 (1976); *Idem*, "Differencing of the Diffusion Equation in LASNEX," Lawrence Livermore National Laboratory, Livermore, CA, UCRL-82747 (1980); *Idem*, *J. Comp. Phys.* **39**, 2, 375 (1981).
16. A. I. Shestakov, J. A. Harte, and D. S. Kershaw, *J. Comp. Phys.* **76**(2),385 (1988).
17. This document describes the electron–ion coupling model in LASNEX: D. C. Eder, "Electron–Ion Coupling in LASNEX," Lawrence Livermore National Laboratory, Livermore, CA, UCID-21544 (1988).
18. D. W. Forslund, J. M. Kindel, and K. Lee, *Phys. Rev. Lett.* **39**, 284 (1977); K. Estabrook and W. L. Kruer, *Phys. Rev. Lett.* **40**, 42 (1978) .
19. D. S. Kershaw, "Interaction of Relativistic Electron Beams with High-Z Plasmas," UCRL-77047 (1975); *Idem*, *Laser Programs Annual Report*, 3–69, Lawrence Livermore National Laboratory, Livermore, CA, UCRL-50021-78 (1978); *Idem*, Lawrence Livermore National Laboratory, Livermore, CA, UCRL-83494 (1979); *Idem*, "Computer Simulation of Suprathermal Transport for Laser Fusion," *Laser Programs Annual Report*, 3–78, Lawrence Livermore National Laboratory, Livermore, CA, UCRL-50021-80 (1980).
20. J. A. Harte and R. M. More, *Laser Programs Annual Report*, 3–66, Lawrence Livermore National Laboratory, Livermore, CA, UCRL-50021-82 (1982).
21. J. A. Harte and D. S. Kershaw, *Laser Programs Annual Report*, 3–63, Lawrence Livermore National Laboratory, Livermore, CA, UCRL-50021-81 (1981).
22. I. J. Feng and R. H. Pratt, "Parameterization of the Bremsstrahlung Spectrum," University of Pittsburgh, Internal Report, PITT–266 (1981); J. A. Harte and Y. T. Lee, *Laser Programs Annual Report*, 3–64, Lawrence Livermore National Laboratory, Livermore, CA, UCRL-50021-82 (1982).
23. M. K. Prasad and D. S. Kershaw, *Phys. Fluids B* **1**, 2430 (1989); *Ibid.*, **3**, 3087 (1991).
24. P. L. Bhatnagar, E. P. Gross, and M. Krook, *Phys. Rev.* **94**, 511 (1954); M. Krook, *J. Fluid Mech.* **6**, 523 (1959).
25. G. Ecker, *Theory of Fully Ionized Plasmas* (Academic Press, New York, NY, 1972); I. P. Shkarofsky, T. W. Johnston, and M. P. Bachynski, *The Particle Kinetic of Plasmas*, (Addison–Wesley, Reading, Massachusettes, 1966).
26. J. F. Luciani, P. Mora, and R. Pellat, *Phys. Fluids* **28**, 835 (1985); J. R. Albritton, E. A. Williams, I. B. Bernstein, and K. P. Swartz, *Phys. Rev. Lett.* **57**, 1887 (1986); M. Prasad, and D. Kershaw, *Phys. Fluids B* **1**, 2430 (1989).
27. R. J. Mason, *J. Comp. Phys.* **71**, 429 (1987); R. J. Mason, "Hybrid and Collisional Implicit Plasma Simulation Models," in *Multiple Time Scales*, J. U. Brackbill and B. I. Cohen, Eds. (Academic Press, Reading, MA, 1985).
28. T. J. M. Boyd and J. J. Sanderson, *Plasma Dynamics* (Barnes & Noble, Inc., New York, NY, 1969).
29. S. I. Braginskii, "Transport Processes in a Plasma," in *Reviews of Plasma Physics*, M. A. Leontovich, Ed. (Consultants Bureau, New York, NY, 1965), vol. 1, p. 205.
30. P. D. Nielsen and G. B. Zimmerman, "Treatment of Theta–Directed Magnetic Fields in LASNEX," Lawrence Livermore National Laboratory, Livermore, CA, UCRL-53123 (1981).
31. J. H. Hammer, Lawrence Livermore National Laboratory, Livermore, CA, private communication (1996).
32. A. I. Shestakov, J. A. Harte, D. S. Kershaw, *J. Comp. Phys.*, **76**, 2, 385 (1988); A. I. Shestakov, "Radiation Diffusion with the Finite-Element Method," *Laser Programs Annual Report*, Lawrence Livermore National Laboratory, Livermore, Ca, UCRL-50021-85 (1985); *Idem*, *Laser Programs Annual Report*, 2–94, Lawrence Livermore National Laboratory, Livermore, CA, UCRL-50021-86 (1986).
33. A. Friedman and D. S. Kershaw, *Laser Programs Annual Report*, 3–68, Lawrence Livermore National Laboratory, Livermore, CA, UCRL-50021-82 (1982).
34. T. S. Axelrod, P. F. Dubois, and C. E. Rhoades, Jr., *J. Comp. Phys.* **54**, 204 (1984).
35. A. Friedman, *Laser Programs Annual Report*, 3–62, Lawrence Livermore National Laboratory, Livermore, CA, UCRL-50021-83 (1983).
36. A. I. Shestakov, D. S. Kershaw, and G. B. Zimmerman, *Nuclear Science and Engineering* **105**, 88 (1990).
37. D. S. Kershaw and M. K. Prasad, *Laser Programs Annual Report*, 2–73, Lawrence Livermore National Laboratory, Livermore, Ca, UCRL-50021-85 (1985).
38. D. S. Kershaw, *Laser Programs Annual Report*, 2–96, Lawrence Livermore National Laboratory, Livermore, CA, UCRL-50021-86 (1986); A. I. Shestakov, D. S. Kershaw, M. K. Prasad, and G. B. Zimmerman, *Ibid.,* 2–89 (1987); A. I. Shestakov, D. S. Kershaw, and M. K. Prasad, *J. Quant. Spectrosc. Radiat. Transfer* **40**(5), 577 (1988).
39. M. K. Prasad, A. I. Shestakov, D. S. Kershaw, and G. B. Zimmerman, *J. Quant, Spectrosc. Radiat. Transfer* **40**(1), 29 (1988).
40. C. D. Levermore, *Discretization Methods for Fokker–Planck Operators*, UCRL-91396 (August 1984).

41. D. S. Kershaw, "Flux Limiting on Nature's Own Way," Lawrence Livermore National Laboratory, Livermore, CA, UCRL-78378 (1976); *Idem*, *Laser Programs Annual Report*, 4–56, Lawrence Livermore National Laboratory, Livermore, CA, UCRL-50021-76 (1976).
42. A. I. Shestakov, J. A. Harte, and D. S. Kershaw, "Solution of the Diffusion Equation by Finite Elements in Lagrangian Hydrodynamic Codes," 2, Lawrence Livermore National Laboratory, Livermore, CA, UCRL-95066 (1986).
43. B. G. Carlson, "The Numerical Theory of Neutron Transport," in *Methods in Computational Physics* (Academic Press, New York, 1963) vol. 1.
44. C. M. Lund and J. R. Wilson, "Some Numerical Methods for Time-Dependent Multifrequency Radiation Transport Calculations in One Dimension," Lawrence Livermore National Laboratory, Livermore, CA, UCRL-84678 (1980).
45. D. S. Kershaw, *Laser Programs Annual Report*, 2–78, Lawrence Livermore National Laboratory, Livermore, CA, UCRL-50021-85 (1985); J. F. Painter, "Finite Element Radiation Transport in One Dimension," Lawrence Livermore National Laboratory, Livermore, CA, UCRL-MI-119254 (1994).
46. A. Friedman, *Laser Programs Annual Report*, 3–51, Lawrence Livermore National Laboratory, Livermore, CA, UCRL-50021-83 (1983); *Idem*, "Calculation of Laser Light Transport on a Lagrangian *R–Z* Mesh," Lawrence Livermore National Laboratory, Livermore, CA, UCRL-93644 (1985).
47. A. B. Langdon, *Phys. Rev. Lett.* **44**, 575 (1980); V. P. Silin, *Sov. Phys.–ETP* **20**, 1510 (1965).
48. Ya. B. Zel'dovich and Yu. P. Raizer, *Physics of Shock Waves and High Temperature Hydrodynamic Phenomena* (Academic Press, New York, NY, 1966) vol. I, chp. V, p. 265; D. Eder, Lawrence Livermore National Laboratory, private communication (1995).
49. D. S. Bailey, *Laser Programs Annual Report*, 2–91, Lawrence Livermore National Laboratory, Livermore, CA, UCRL-50021-75 (1975).
50. K. Estabrook, J. Harte, and D. Bailey, *Laser Programs Annual Report*, 3–31, Lawrence Livermore National Laboratory, Livermore, CA, UCRL-50021-78 (1978).
51. A. Friedman and E. A. Williams, *Laser Programs Annual Report*, 3–61, Lawrence Livermore National Laboratory, Livermore, CA, UCRL-50021-84 (1984).
52. J. Harte, *Laser Programs Annual Report*, 4–31, Lawrence Livermore National Laboratory, Livermore, CA, UCRL-50021-77 (1977); J. Harte and G. Zimmerman, "Ponderomotive Force in a Hydrodynamic Simulation Code," Lawrence Livermore National Laboratory, Livermore, CA, UCRL-79860 (1977).
53. M. K. Prasad, Lawrence Livermore National Laboratory, Livermore, CA, private communication.
54. R. M. More and D. S. Bailey, *Laser Programs Annual Report*, 2–72, Lawrence Livermore National Laboratory, Livermore, CA, UCRL-50021-79 (1979).
55. D. S. Bailey, Y. T. Lee, and R. M. More, *Laser Programs Annual Report*, 3–64, Lawrence Livermore National Laboratory, Livermore, CA, UCRL-50021-81 (1981).
56. A. I. Shestakov, Lawrence Livermore National Laboratory, Livermore, CA, private communication.
57. W. E. Alley, *ICF Quarterly Report* **2**(4), 160–165, Lawrence Livermore National Laboratory, Livermore, CA, UCRL-LR-105821-92-4 (1993).
58. R. M. White, D. A. Resler, and S. I. Warshaw, "Evaluation of Charged–Particle Reactions for Fusion Applications," *Proc. of the Int'l. Conf. Nuclear Data for Science and Technology*, S. M. Qaim, Ed. (Julich, Germany, 1991) p. 834; M. J. Harris, W. A. Fowler, G. R. Caughlan, and B. A. Zimmerman, *Ann. Rev. Astron. Astrophys.* **21**, 165 (1983); G. B. Zimmerman, *Laser Programs Annual Report*, 3–64, Lawrence Livermore National Laboratory, Livermore, CA, UCRL-50021-83 (1983).
59. R. J. Howerton, R. E. Dye, and S. T. Perkins, "Evaluated Nuclear Data Library," Lawrence Livermore National Laboratory, Livermore, CA, UCRL-50400, vol. 4, Rev. 1 (1981) .
60. D. E. Cullen, M. H. Chen, J. H. Hubbell, S. T. Perkins, E. F. Plechaty, J. A. Rathkopf, and J. H. Scofield, "Tables and Graphs of Photon-Interaction Cross Sections from 10 eV to 100 GeV Derived from the LLNL Evaluated Photon Data Library (EPDL)," Lawrence Livermore National Laboratory, Livermore, CA, UCRL-50400, vol. 6, Rev. 4 (1989).
61. C. D. Levermore and G. C. Pomraning, *The Astrophysical Journal* **248**, 321 (1981).
62. G. B. Zimmerman, *Laser Programs Annual Report*, 3–76, Lawrence Livermore National Laboratory, Livermore, CA, UCRL-50021-79 (1979); E. G. Corman, W. E. Loewe, G. E. Cooper, and A. M. M. Winslow, *Nuclear Fusion* **15**, 377 (1975).
63. G. B. Zimmerman, "Recent Developments in Monte Carlo Techniques," 6–7, Lawrence Livermore National Laboratory, Livermore, CA, UCRL-JC-105616 (1990).
64. P. D. Nielsen and G. B. Zimmerman, "Treatment of Theta-Directed Magnetic Fields in LASNEX," Lawrence Livermore National Laboratory, Livermore, CA, UCRL-53123 (1981); P. D. Nielsen, "A Computational Investigation of the Limits to Pease–Braginskii Collapse of a Z-Pinch," Lawrence Livermore National Laboratory, Livermore, CA, UCRL-53166 ((Ph.D. Thesis, 1981).
65. J. H. Hammer, J. L. Eddleman, P. T. Springer, M. Tabak, A. Toor, K. L. Wong, G. B. Zimmerman, C. Deeney, R. Humphreys, T. J. Nash, T. W. L. Sanford, R. B. Spielman, and J. S. De Groot, *Phys. Plasmas* **3**, 2063 (1996).
66. S. Maxon, J. H. Hammer, J. L. Eddleman, M. Tabak, G. B. Zimmerman, W. E. Alley, K. G. Estabrook, J. A. Harte, T. J. Nash, T. W. L. Sanford, and J. S. De Groot, *Phys. Plasmas* **3**, 1737 (1996).
67. "Sesame: The LANL EOS Database," S. P. Lyon and J. D. Johnson, Eds., LANL, Los Alamos, NM, LA-UR-92-3407 (1992).
68. R. M. More and G. B. Zimmerman, *Laser Programs Annual Report*, 3–55, Lawrence Livermore National Laboratory, Livermore, CA, UCRL-50021-83 (1983); R. M. More, K. H. Warren, D. A. Young, and G. B. Zimmerman, *Phys. Fluids* **31**, 3059 (1988); D. A. Young and E. Corey, *J. Appl. Physics* **78**, 3748 (1995).
69. J. Abdallah and B. E. H. Clark, Los Alamos National Laboratory, Los Alamos, NM, private communication (1994).
70. C. Iglesias, B. Wilson, and J. Harte, Lawrence Livermore National Laboratory, Livermore, CA, private communication (1996)
71. S. A. Brown and D. Braddy, "PACT Users' Guide," Lawrence Livermore National Laboratory, Livermore, CA, UCRL-MA-112087 (1995).
72. W. A. Lokke and W. Grasberger, "XSNQ-U: A Non-LTE Emission and Absorption Coefficient Subroutine," Lawrence Livermore National Laboratory, Livermore, CA, UCRL-52276 (1977); G. Pollak, "Detailed Physics of XSN-U Opacity Package," LANL, Los Alamos, NM, LA-UR-90-2423 (1990).
73. G. B. Zimmerman and R. M. More, *J. Quant. Spectrosc. Radiat. Transfer* **23**, 517 (1979).
74. W. E. Alley, Lawrence Livermore National Laboratory, Livermore, CA, private communication (1995).
75. D. A. Liberman, J. R. Albritton, B. G. Wilson, and W. E. Alley, *Phys. Rev. A* **50**, 171 (1994).
76. Y. T. Lee, G. B. Zimmerman, D. S. Bailey, D. Dickson, and D. Kim, "A Time-Dependent Ionization Balance Model for Non-LTE Plasma," Lawrence Livermore National Laboratory, Livermore, CA, UCRL-95149; Y. T. Lee, *J. Quant. Spectrosc. Radiat. Transfer* **38**, 131 (1987).
77. Y. T. Lee, R. A. London, and G. B. Zimmerman, *Phys. Fluids B* **2**, 2731 (1990); A. I. Shestakov and D. C. Eder, *J. Quant. Spectrosc. Radiat. Transfer* **42**, 483 (1989).

78. J. C. Stewart and K. D. Pyatt, *Ap. J.* **144**, 1204 (1966).
79. B. C. Stuart, M. D. Feit, A. M. Rubenchik, B. W. Shore, and M. D. Perry, *Phys. Rev. Lett.* **74**, 2248 (1995).
80. P. F. Dubois, *Computers in Physics* **8** (1), Jan./Feb. 1994; L. Busby, P. F. Dubois, S. Wilson, *ICF Quarterly Report* **3**(1), 50 Lawrence Livermore National Laboratory, Livermore, CA, UCRL-LR-105521-93-1(1993).
81. L. Suter, Lawrence Livermore National Laboratory, Livermore, CA, veteran LASNEX user, private communication (1996).
82. B. A. Remington, S. V. Weber, S. W. Haan, J. D. Kilkenny, S. G. Glendinning, R. J. Wallace, W. H. Goldstein, B. G. Wilson, and J. K. Nash, *Phys. Fluids B* **5**, 2589 (1993) .
83. S. Chandarsekhar, *Hydrodynamic and Hydromagnetic Stability* (Oxford University Press, London, 1968), Ch. 10.
84. S. W. Haan, Lawrence Livermore National Laboratory, Livermore, CA, private communication (1996).
85. M. M. Marinak, Lawrence Livermore National Laboratory, Livermore, CA, private communication (1996).
86. T. R. Dittrich, B. A. Hammel, C. J. Keane, R. McEachern, R. E. Turner, S. W. Haan, and L. J. Suter, *Phy. Rev. Lett.* **74**, 2324 (1994).
87. S. W. Haan, *Phys. Rev. A* **39**, 5812 (1989).